Desalination and Water Treatment
www.deswater.com

doi: 10.5004/dwt.2017.21201

84 (2017) 123–134
July

Experimental modeling of an air-gap membrane distillation module and simulation of a solar thermal integrated system for water purification

N.T. Uday Kumar[a,b,*], Andrew Martin[b]

[a]*RAK Research and Innovation Center, American University of Ras Al Khaimah (AURAK), Ras Al Khaimah, UAE, emails: uday.kumar@aurak.ac.ae (N.T. Uday Kumar), andrew.martin@energy.kth.se (A. Martin)*
[b]*Department of Energy Technology, KTH Royal Institute of Technology, Stockholm, Sweden*

Received 25 January 2017; Accepted 12 July 2017

ABSTRACT

Membrane distillation is a novel process that could be adapted effectively for many water purification applications. In recent years, several bench, pilot and commercial scale membrane distillation systems with production capacities ranging from 20 L/d to 50 m^3/d were developed and tested. In this work, a single cassette air-gap membrane distillation (AGMD) module was characterized to identify the effect of process parameters on distillate flux and thermal efficiency. Favorable conditions to obtain distillate flow rate of 1.5–3 kg/h were determined on a bench scale experimental setup. Factorial design of experiments was conducted and response surface methodology (RSM) was applied to develop an empirical regression model relating operating parameters with AGMD system performance indicators. Operating parameters including hot feed inlet temperature (T_{Hin}), cold feed inlet temperature (T_{Cin}), feed flow rate (V_f) and feed conductivity (C_f) were considered. Distillate flux (J_d) and specific performance ratio (SPR) were selected as the performance indicators for the modeling. The developed regression model using RSM was tested by analysis of variance. Regression analysis showed agreement with the experimental data fitted with second-order polynomial model having determination coefficient (R^2) values of 0.996 and 0.941 for J_d and SPR, respectively. Numerical optimization has been carried out to identify optimal set of operating conditions for achieving desired operation. Also, dynamic simulation of the membrane distillation module integrated solar thermal system has been reported along with validation of the system model by comparing with the experimental data obtained from a pilot scale setup located in UAE.

Keywords: AGMD; Factorial design; Response surface methodology; ANOVA; Solar membrane distillation

1. Introduction

Employing distillation process in water purification has distinct advantages over other conventional membrane separating processes, in particular concerning separation efficiency: such processes can theoretically remove or destroy all pathogens and remove all minerals, while volatile organic compounds can be stripped. Membrane distillation (MD) is a novel process combining distillation and membrane separation that could be adapted effectively for many water purification applications. MD is a thermally driven process in which the driving force is the vapor pressure difference between the hot and cold side. Water is (usually) the major component present in the feed solution, which vaporizes and pass through a microporous hydrophobic membrane. The liquid feed to be treated by MD should be maintained in direct contact with one side of the membrane without penetrating its dry pores at normal operating temperatures of less than 80°C [1]. Membranes made using polypropylene (PP), polyvinylidene fluoride and polytetrafluoroethylene (PTFE) materials were used in most of the MD processes [2]. Compared with conventional separating process, MD has distinct advantages of low operating temperature and pressure, tolerance to varying salt concentrations and able to

* Corresponding author.

use low grade or waste heat [3]. Based on the various modes of vapor condensation in the cold side, MD process can be divided into direct contact membrane distillation (DCMD), air-gap membrane distillation (AGMD), vacuum membrane distillation (VMD), and sweep gas membrane distillation (SGMD). DCMD is the most studied MD configuration due to simplicity and ease of handling. However, energy efficiency is low for DCMD due to conduction heat losses. A stagnant air gap is interposed between the membrane and a condensation surface as in the case of AGMD, increases the thermal energy efficiency of the process inherently [4]. However, various issues related to high specific thermal energy consumption, membrane development specific for AGMD operation and also efficient module designs need to be addressed for efficient operation of AGMD. Hence, apart from the conventional AGMD processes, various configurations have been developed by researchers namely liquid gap MD, material gap MD, permeate gap MD and conductive gap MD [5–7].

In spite of latest advancements in AGMD configurations, most of the commercial/semi-commercial MD systems operated in the world constitute of AGMD technique. Dated back to 1988, a first flat plate AGMD system developed by the Swedish Svenska Utvecklings AB [8]. Today such modules are manufactured and commercialized by Scarab Development. Each module is made up of 10 planar cassettes with an overall membrane surface of 2.3 m^2 and a global capacity of 1–2 m^3/d of distillate water. The single stage consists of injection molded plastic frames containing two parallel membranes, feed and exit channels for the warm water and two condensing walls [9]. Kullab et al. [10] modified the Scarab AGMD modules for improving thermal efficiency of the modules. Hanemaaijer et al. [11] developed a multistage AGMD system both with hollow fiber and plate-and-frame configurations. This unit has been labelled as Memstill and two pilot plants have been installed and characterized by design capacities equal to 50 and 80 m^3/d, respectively [12]. To increase the thermal efficiency, spiral wound MD modules were developed by Fraunhofer ISE operated with production capacity of 100 L/d and extended to 500 L/d to 10 m^3/d through multiple modules [13,14,15]. However, many of these modules were designed for desalination at production capacities greater than 100 L/d whereas present study utilizes AGMD module which is tested for low capacity production focusing on household applications [16]. Khan et al. conducted experimental analysis from arsenic removal using single cassette AGMD with effective membrane area of 0.2 m^2 and reported fluxes of 20 L/m^2 h at a temperature difference of 50°C between hot and cold inlet temperatures [17]. However, complete parametric characterization has not been reported in the literature for these single cassette MD modules which forms the main focus of the present study.

In conventional experimental modeling one of the parameter is changed, while the other parameters are kept constant in order to evaluate the impact on the system performance. In order to reveal complex interaction between the system parameters, which are kept hidden using conventional experiments, design of experiments (DoE) approach would be employed [18]. Factorial design is a technique where each input parameter is changed in steps, called levels and a low order polynomial is fit as an approximation of the relation of the experimental response and the independent variables. A commonly used visualization technique is the response surface methodology (RSM), where the predicted response is plotted in as a function of two of the inputs that allows to visualize interactions between them. Khayet et al. [19] applied factorial design and RSM models for DCMD to optimize the flux by changing the flow rates, mean temperature and initial salt concentrations. Model predictions performed on four different membranes were evaluated as satisfactory compared with the experimental data using the coefficient of determination R^2. Khayet and Cojocaru [20] modeled and optimized an AGMD process used in desalination. Regression models have been developed to predict the performance index and the specific performance index that takes into consideration the energy consumption as a function of different variables. He et al. [21] applied factorial design and RSM to analyze the relationships between operating parameters (hot and cold inlet temperatures, feed flow rate) on performance indicators including distillate flux and gained output index of a hollow fiber AGMD module. Onsekizoglu et al. [22] applied RSM for osmotic MD to model the behavior of flux and dissolved solid content as a function of osmotic agent concentration, flow rates and temperature differences between the feed and the permeate. Mohammadi and Safavi [23] used the Taguchi method which is an advanced DoE technique to optimize the performance of VMD using the parameters; feed flow rates and temperatures, vacuum pressures and inlet concentrations. The Taguchi method minimizes the amount of experiments needed for the modeling. Khayet et al. [24] also applied factorial design and RSM to optimize the flux of an SGMD system by changing the water and sweep gas inlet temperatures and circulation velocities.

Literature study shows that simple empirical models could be developed through experimental data using DoE approach. In the present work, a single cassette AGMD module is characterized experimentally and thermal performance was evaluated. Effect of various input parameters such as inlet temperatures in hot and cold channels of the MD module, feed flow rate and conductivity on the distillated flux has been analyzed through experiments. Further to analyze interaction between operational parameters, factorial DoE was conducted and RSM was applied. The developed RSM regression model was tested by analysis of variance (ANOVA) and validated using experimental results. Parametric optimization has been carried out as well to identify suitable conditions for operating MD with constant or dynamic energy supply (e.g. solar thermal energy).

Dynamic transient system simulation (TRNSYS) tool was used in our previous studies to simulate large cassette MD modules for co-generation and polygeneration applications [25,26]. Similarly, present work focuses on simulating solar thermal driven membrane distillation (SMD) system utilizing the RSM model as a component for dynamic analysis. Simulation results have been validated with experimental data obtained from a pilot scale SMD system installed in UAE [27].

2. Bench scale experimental setup and methodology

2.1. Flat sheet AGMD module

The present work utilizes a bench scale AGMD unit with a single membrane cassette developed in collaboration with

an industrial research partner [28]. Fig. 1 shows the layout of components in the bench scale MD module and also shows the picture of the module fitted with the cassette in a plate and frame configuration. Specifications of the membrane cassette are:

- Material: hydrophobic PTFE membrane.
- Pore size: 0.2 μm; thickness: 280 μm; total membrane area: 0.2 m^2.

The AGMD module consists of a gap of 2.4 cm between two aluminum condensing plates, behind which are located the cooling channels in a serpentine shape covered with rigid aluminum end plates. Two membranes each of 0.1 m^2 surface area are thermally welded on to a PP cassette frame to fit into the module. The hot feed flow comes in from the bottom of the cassette, and flows out from the top outlet located on the same side as inlet. Sufficient baffles are provided two separate hot feed into two channels toward the two membranes attached. An air-gap of around 5 mm is maintained on both sides. However, when the cassette is filled with feed, the membranes bulge out onto the condensation plates and the gap reduces to as low as 1 mm. The gap was maintained using a plastic spacer between membrane and condensation plate.

The whole process can be summarized through description of flows in three channels:

- Hot channel, where hot feed enters the cassette in contact with the membrane, vapor is generated and passes through membrane.
- Air-gap, a stagnant air gap between outer membrane surface and condensation plates allow the vapor to condense and collected in a distillate channel at the bottom.
- Cold channel, where a cold fluid flows in contact with other side of condensation plate absorbs the latent heat of condensed vapors.

2.2. Experimental setup and thermal performance

A bench scale experimental setup as shown in Fig. 2 is designed for characterization of MD performance. The setup consists of a single cassette AGMD module connected with hot and cold water storage tanks. Feedwater is taken from the municipal water supply and filled into a 20 L insulated stainless steel tank. For feedwater with higher concentrations, seawater is diluted to the desired concentration levels for experimentation. Storage tank is fitted with a thermostat controlled electric heating elements on both sides to maintain hot feed temperatures for controlled experiments. Since the tap cold water temperatures are below 10°C, cold loop is designed in such way to experiment at high cold water temperatures. A large buffer tank of 1 m^3 capacity is used to store hot water and the heat is exchanged with cold water from the taps using a plate heat exchanger. A thermostatic mixing valve is used to control temperatures on cold side and manual valves to control flow on cold side. Temperatures, feed flows, feed and distillate conductivities are monitored and recorded using a data logger.

Performance index (PR) was used to evaluate performance of AGMD and plotted as a function of temperature differences on hot and cold channels [29]. The PR is calculated as:

$$PR = \frac{\lambda.\rho_w\left(T_d, P_a\right).V_d}{Q_{md}} \quad (1)$$

where λ is the water latent heat of vaporization (2,326 kJ/kg), V_d is the distillate volumetric flow rate, ρ_w is the water density as a function of the distillate temperature and atmospheric pressure, Q_{md} is the thermal energy supplied to the system calculated using the energy balance equations:

$$Q_{md} = V'.[\rho_w(T_{Hin}, P_{Hin}).h_w(T_{Hin}, P_{Hin}) - \rho_w(T_{Hout}, P_{Hout}).h_w(T_{Hout}, P_{Hout})] \quad (2)$$

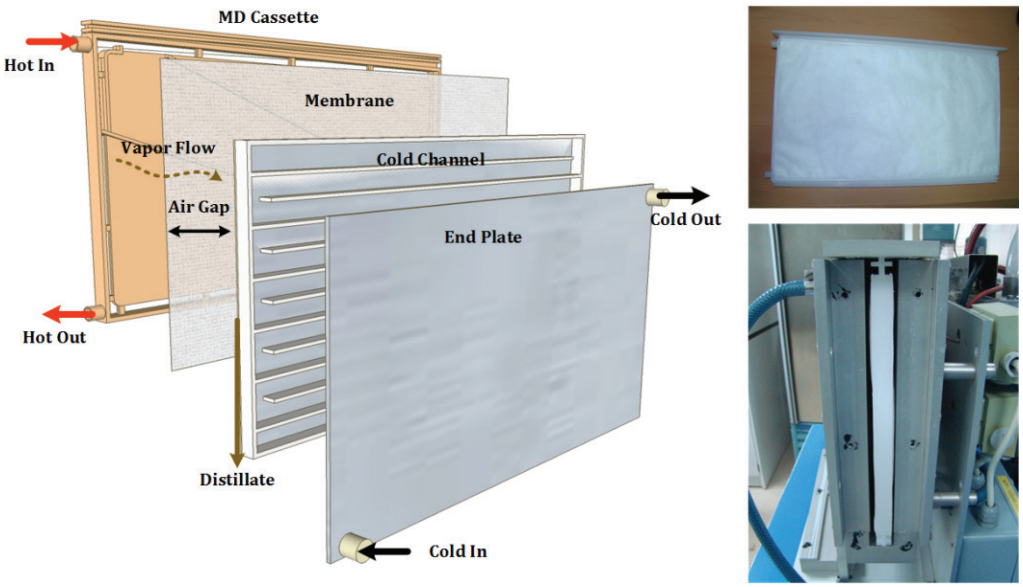

Fig. 1. Bench scale MD module and pictures of cassette fitted into module.

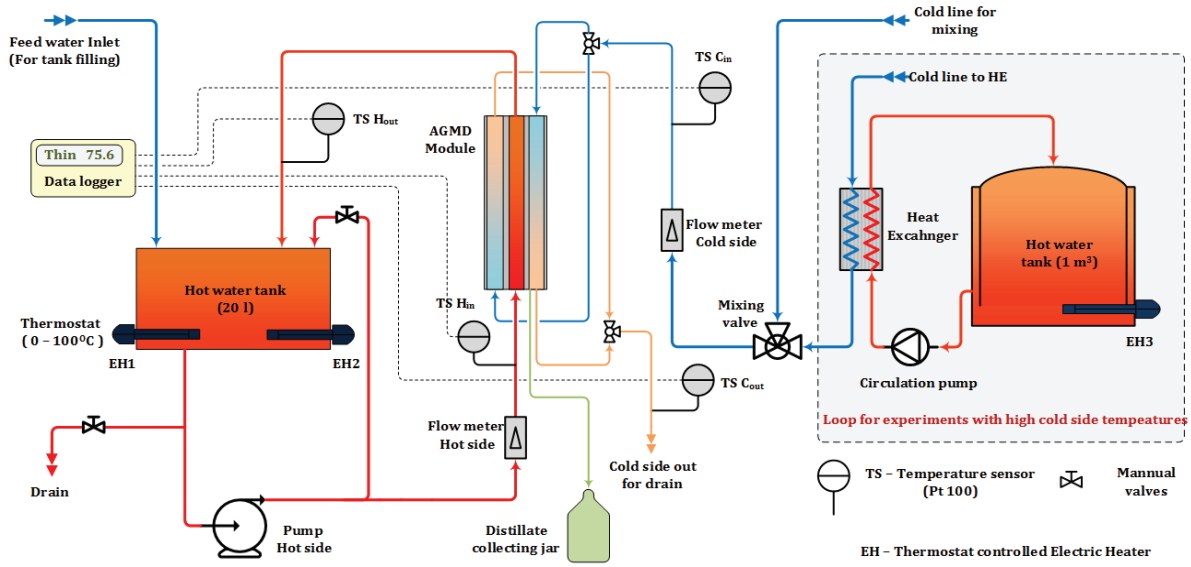

Fig. 2. Schematic diagram of laboratory scale experimental setup.

where $V' = V_f - V_d$ and V_f is the feed flow rate to the MD module.

2.3. Empirical modeling of AGMD system

RSM that involves statistical DoE in which all factors are varied simultaneously is a possible method permitting to study the interaction effects between parameters and to model and optimize the AGMD process. The DoE and RSM were employed in this study for modeling and to obtain optimum conditions of AGMD module. The procedure of DoE and RSM consists of the following steps:

- Designing and conducting a series of experiments to obtain the performance indicators.
- Developing mathematical models of first- or second-order response surface with best fittings.
- Studying effects of the process variables on the responses using 2D and/or 3D plots.
- Finding out optimal set of process variables that guarantee an optimum value of selected response.

The most significant design variables that affect the AGMD performance are the feed inlet temperature (T_{Hin}), the cooling inlet temperature (T_{Cin}), that is, condensation temperature, the feed flow rate (V_f) and feed concentration (C_f). The selected performance indicators of the AGMD process are distillate flux (J_d) and specific performance ratio (SPR). J_d is calculated by:

$$J_d = \frac{M_d}{S.t} \tag{3}$$

where M_d (kg) is the mass of distillate water collected within the time t, and S (m²) is the effective membrane surface area of evaporation. SPR is obtained by:

$$\text{SPR} = \frac{M_d}{Q_{md}} \tag{4}$$

Table 1
Operational conditions of tested AGMD module

Operational parameter	Specification
Feed flow rate, L/min	4, 6 and 8
Hot water operation temperature, °C	40–80
Cold water operation temperature, °C	10–50
Tap water conductivity, μS/cm	500–10,000

where Q_{md} (kWh) is the thermal energy supplied to the AGMD module which is calculated using Eq. (2) mentioned in previous section. Since SPR is the function of J_d, T_{Hin}, V_f, C_f and T_{Hout}, which involves both the inputs and the outputs of the AGMD system. A relationship between the system outputs (J_d and T_{Hout}) with system inputs (T_{Cin}, T_{Hin}, V_f and C_f) was established first and then the SPR was obtained for the given inputs. The DoE, ANOVA and response surface model regression analysis were carried out by using Design Expert 10 [30].

3. Results and discussion

3.1. Characterization experiments

Thorough experimental campaign was carried out to analyze the effect of important parameters on distillate flux namely feed inlet temperatures on hot and cold sides, hot side feed flow rate and feed concentrations as per the specifications shown in Table 1. Manufacturer recommended operational values were used during experimentation and some of them were varied and others were surpassed, namely maximum pressure. The module materials can stand higher temperatures but they are sensitive to pressure on hot side of membrane, for that reason flow rate could only be varied between the specified ranges (4–8 L/min). A set of preliminary experiments have been performed with municipal tap water as feed and pure distillate was obtained at conductivities less than 5 μS/cm. Experiments were further extended

with higher feed concentrations and pure distillate was obtained with conductivities less than 20 μS/cm. Salt rejection factor of more than 99.9% was obtained during all experiments. Each experiment was conducted for 3 h and repeated twice to obtain an average value from all three experiments. The uncertainty in actual temperature measurements was estimated to be ±0.2°C for the sensors used with a standard deviation of 0.05°C. For MD feed flow rate measurements, the standard deviation was less than 0.3 kg/h and measured flow difference from the set point was less than ±1.5 kg/h. An overall uncertainty of approximately ±10 g/h was determined for weight measurement of the distillate collected.

Both hot and cold side temperatures have significant effects on distillate flux. Researchers [31] reported that effect of hot side temperatures were dominant compared with cold side. Fig. 3 shows the combined effect of changing feed evaporator temperature and coolant temperature from the experimental results. For the feed flow rate of 6 L/min, flux varies from 0.1 to 24 kg/h m^2. It is evident that with increase and decrease of evaporator and coolant temperatures, respectively, the water production rate increases. This was due to dominance of MD process by the difference in vapor pressure, which is expressed in terms of temperature by an exponential variation in Antoine's equation. For the same temperature difference delta T ($T_{Hin} - T_{Cin}$), the difference of vapor pressure have different values depending on feed or coolant temperature and hence production varies.

Fig. 4 shows the effect of feed flow rate on distillate flux at different hot inlet temperatures for a constant cold inlet temperature of 30°C. Plot indicates a slight increase in distillate flux within the investigated flow rate range and the increase is not significant at low hot inlet temperatures. However, at high feed inlet temperature better mixing of fluid could be obtained with increased feed flow and hence significant increase in flux is observed. Plot also shows remarkable influence of hot feed temperature on the distillate flux, which is enhanced by a factor 6–7 varying T_{Hin} from 40°C to 80°C.

As shown in Fig. 5, the performance ratio of the system decreases with increase in cold inlet temperatures and increases with delta T ($T_{Hin} - T_{Cin}$). No heat recovery was employed in the process and hence PR values are less than 1. The PR values for a feed flow rate of 6 L/min varied from 0.6 to 0.8 which were in agreement with values reported in the literature for the large MD modules utilizing similar membranes [32]. Specific thermal energy consumption (STEC), which is the thermal energy consumed to produce 1 kg of pure distillate is plotted against feed flow rate in Fig. 6. Results show a linear response to flow rate and decreases with increases in the hot side absolute temperature. These dependencies are obvious due to increase in thermal capacity of feed stream and increase in distillate production, which leads to reduced specific consumption values. By doubling the hot flow rate, STEC increases by 25%–35% depending on the hot inlet temperatures. At cold inlet temperature of 30°C specific consumption ranges from 700 to 1,100 kWh/m^3 of distillate produced.

3.2. Response surface model and ANOVA

The central composite design (CCD) of orthogonal type was employed in this study to carry out the AGMD experiments. For modeling purpose, the variables were coded as

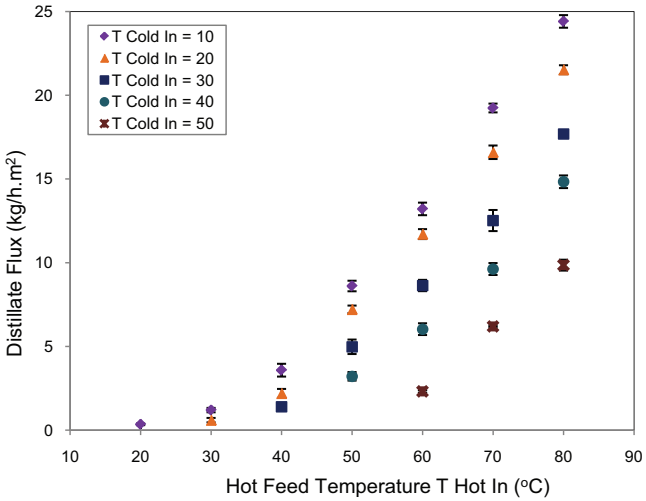

Fig. 3. Effect feed inlet temperatures on distillate flux (feed flow V_f = 6 L/min).

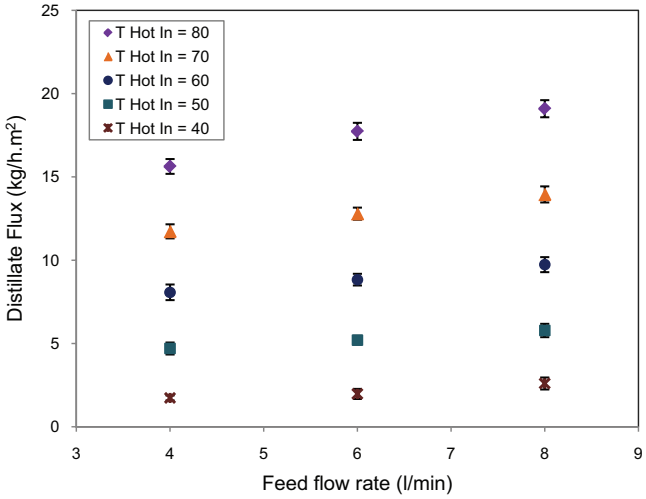

Fig. 4. Effect of feed flow rate on distillate flux (T_{Cin} = 30°C).

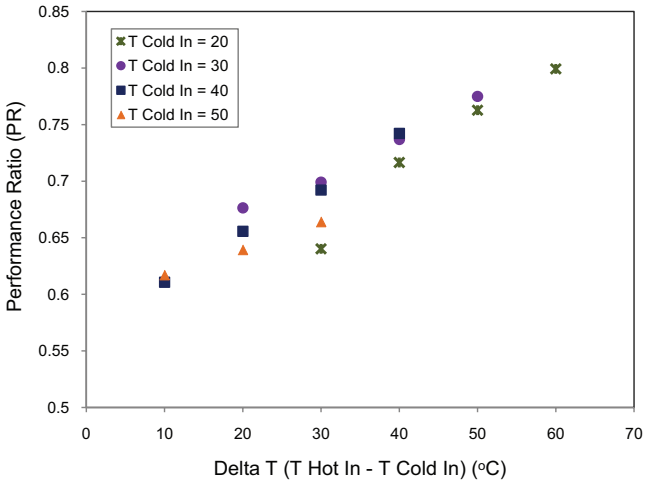

Fig. 5. Performance ratio as a function of delta T ($T_{Hin} - T_{Cin}$).

shown in Table 2. According to CCD, a total number of 25 experiments have been performed and the operating conditions are summarized in Table 3. The first 16 experiments runs correspond to the orthogonal design, the next experiments (runs 17–24) are the axial experiments with "star points" to form the CCD and finally the last experiment (run 25) is replicate point to estimate the experimental error. Each run has been performed thrice for 3 h and data were obtained for mean permeate flux (J_d) along with hot feed outlet temperatures (T_{Hout}) and MD energy consumption (Q_{md}). It was observed that during all experimental runs the salt rejection factor is more than 99% and hence the dependence of feed concentration on distillate flux was not significant compared with other variables considered for RSM model.

The selected responses for RSM were listed in Table 3. The "fit summary" reports generated by Design Expert recommended that the quadratic regression model based on two-factor interaction method (2FI) was suitable to describe the relationships between the inputs and the three responses. The regression quadratic model with coded parameters can be expressed as:

$$Y = \beta_0 + \beta_1 X_1 + \beta_2 X_2 + \beta_3 X_3 + \beta_{12} X_1 X_2 + \beta_{13} X_1 X_3 + \beta_{23} X_2 X_3 + \beta_{11} X_1^2 + \beta_{22} X_2^2 + \beta_{33} X_3^2 \quad (5)$$

The significance of the regression coefficients of the models written as a function of the coded variables was tested using the statistical Student's *t*-test including only the significant terms in all equations. The statistical validation of the RSM was performed by means of ANOVA presented in Table 4 for the responses J_d and T_{Hout} and further the response SPR was determined. According to the ANOVA results of the two responses, the *F* values are quite high and the *P* values are smaller than 0.0001. From this view point, we conclude that T_{Cin}, T_{Hin}, V_f and interaction between all these variables are significant variances for the response J_d, and for response T_{Hout} the significant variances are T_{Cin}, T_{Hin}, V_f and interaction of T_{Cin} and T_{Hin}. After ignoring the statistically non-significant terms, the final regression equations for J_d and T_{Hout} in terms of actual operating parameters were determined as follows:

$$J_d = -6.57 + 0.16 \times T_{Cin} + 0.15 \times T_{Hin} - 5.86 \times 10^{-3} \times V_f - 5.77 \times 10^{-3} \times T_{Cin} T_{Hin} - 2.5 \times 10^{-4} \times T_{Cin} V_f + 3.44 \times 10^{-4} \times T_{Hin} V_f + 2.48 \times 10^{-3} \times T_{Hin}^2 \quad (6)$$

$$T_{Hout} = 3.097 + 6.82 \times 10^{-2} \times T_{Cin} + 0.772 \times T_{Hin} + 3.5 \times 10^{-3} \times V_f + 1.42 \times 10^{-3} \times T_{Cin} T_{Hin} \quad (7)$$

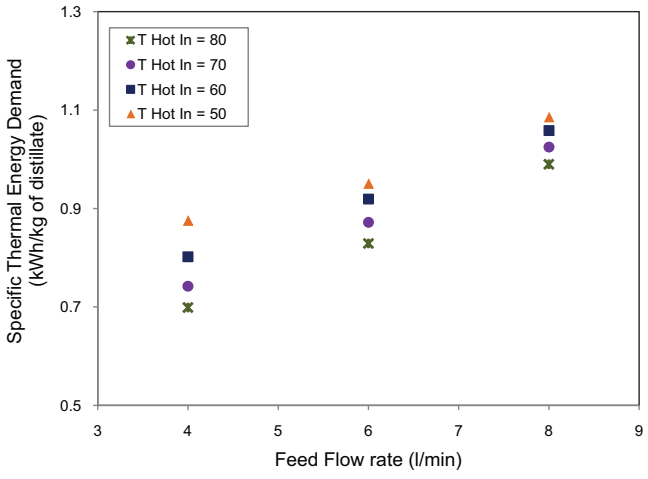

Fig. 6. Specific thermal energy consumption with flow rate.

Experimental results from characterization studies were compared with predicted response values in order to confirm the adequacy of the regression model. J_d and SPR values observed from experiments and predicted by RSM were compared as shown in Fig. 7. The experimental and predicted values show good agreement confirming the validity of the regression model. As shown in Fig. 7, the R^2 value of 0.99 for the distillate flux was obtained which is in agreement with the adjusted coefficient of determination $R^2_{Adjusted}$ indicating that the model explains 99% of the variability of this response (J_d). For the SPR, the R^2 value is 0.94. This indicates that the model explains 94% of the variability of the response SPR. Therefore, all the obtained statistical estimators reveal that the developed mathematical models are statistically valid for the prediction of responses for pure water production using the bench scale AGMD module.

Fig. 8 shows three dimensional plots (3D) of the surfaces showing mutual effects of two factors while fixing the third factor and their influence upon the responses distillate flux (J_d) and SPR. The influence of cold feed inlet temperature (T_{Cin}), hot feed inlet temperature (T_{Hin}) and feed flow rate (V_f) on distillate flux (J_d) was presented in Figs. 8(a1), (b1) and (c1). It can be seen that J_d increased significantly with increasing T_{Hin}. This is due to the fact that the exponential increase of the equilibrium vapor pressure of the feed solution with

Table 2
Design parameters and the actual values of the coded level used for AGMD experiments

Design parameters	Coded parameters	Actual values of coded levels				
		$-\alpha$[a]	−1	0	+1	$+\alpha$
Cold inlet temperature, T_{Cin} (°C)	X_1	8.8	15	30	45	51.2
Hot inlet temperature, T_{Hin} (°C)	X_2	43.8	50	65	80	86.2
Feed flow rate, V_f (kg/h)	X_3	190	240	360	480	504
Feed conductivity, C_f (mS/cm)	X_4	0.86	1	5.5	10	11.8

[a]α = 1.4142 (starting point for CCD of orthogonal type with four variables).

Table 3
Results of CCD and the experiments

Run	Variable X_1 (T_{Cin})		Variable X_2 (T_{Hin})		Variable X_3 (V_f)		Variable X_4 (C_f)		Response J_d (kg/h m^2)		Response SPR (kg/kWh)	
	Coded	Actual	Coded	Actual	Coded	Actual	Coded	Actual	Model	Deviation %	Model	Deviation %
1	–1	15	–1	50	–1	240	–1	1	7.12	0.1	1.039	1.0
2	1	45	–1	50	–1	240	–1	1	1.49	7.2	0.858	5.1
3	–1	15	1	80	–1	240	–1	1	21.23	1.6	1.471	2.1
4	1	45	1	80	–1	240	–1	1	10.40	3.7	1.300	10.8
5	–1	15	–1	50	1	480	–1	1	8.94	1.0	0.787	2.6
6	1	45	–1	50	1	480	–1	1	1.51	13.6	1.286	5.1
7	–1	15	1	80	1	480	–1	1	25.52	2.0	0.948	2.5
8	1	45	1	80	1	480	–1	1	12.90	3.3	0.926	2.6
9	–1	15	–1	50	–1	240	1	10	7.12	5.3	1.048	5.1
10	1	45	–1	50	–1	240	1	10	1.49	4.4	0.877	0.0
11	–1	15	1	80	–1	240	1	10	21.23	1.5	1.476	12.5
12	1	45	1	80	–1	240	1	10	10.40	2.7	1.303	1.8
13	–1	15	–1	50	1	480	1	10	8.94	4.1	0.796	3.5
14	1	45	–1	50	1	480	1	10	1.51	11.0	1.280	2.8
15	–1	15	1	80	1	480	1	10	25.52	1.0	0.930	0.9
16	1	45	1	80	1	480	1	10	12.90	2.4	0.929	1.3
17	–α	8.8	0	65	0	360	0	5.5	17.03	7.2	0.848	4.1
18	+α	51.2	0	65	0	360	0	5.5	4.13	14.4	1.277	5.2
19	0	30	–α	43.8	0	360	0	5.5	2.69	8.9	0.610	3.6
20	0	30	+α	86.2	0	360	0	5.5	20.71	4.0	1.026	5.1
21	0	30	0	65	–α	190	0	5.5	9.05	0.0	1.529	1.1
22	0	30	0	65	+α	530	0	5.5	12.11	4.1	0.884	2.8
23	0	30	0	65	0	360	–α	0.86	10.58	0.6	1.115	5.0
24	0	30	0	65	0	360	+α	11.8	10.58	6.4	0.965	5.4
25	0	30	0	65	0	360	0	5.5	10.58	1.8	1.073	4.9

Table 4
Analysis of variance (ANOVA) of the RSM model corresponding to the response

Response	Source	Degrees of freedom	Sum of squares	Mean of squares	*F* Value	*P* Value	R^2	$R^2_{Adjusted}$
Flux J_d (kg/h m^2)	Model	7	1,295.54	185.08	653.17	<0.0001	0.9963	0.9948
	Residual	17	4.82	0.28				
	Total	24	1,300.35					
T_{Hout} (°C)	Model	4	3,110.68	777.67	2,155.71	<0.0001	0.9977	0.9972
	Residual	20	7.21	0.36				
	Total	24	3,117.9					

the increase of temperature. Therefore, the increase of T_{Hin} enlarges the driving force of the transmembrane mass transfer. On the other hand, the decrease in response J_d is also significant with increase in T_{Cin}. As we know that the driving force for transmembrane mass transfer is the temperature gradient between the membrane surface and the dense condensing wall, when higher T_{Cin} is applied distillate flux J_d decreases. On the other hand, increasing V_f had a positive effect on distillate flux. When feed flow increases, the boundary layer become thinner enabling proper mixing of the fluid in the module which increases the driving force for the AGMD process. From the figure, it is apparent that T_{Hin} has the most significant effect on J_d followed by T_{Cin} and V_f. Moreover, the 3D surface plots of J_d also show the significance of interaction effects of every two input variables.

The effects of operating parameters (T_{Cin}, T_{Hin} and V_f) on SPR are shown in Figs. 8(a2), (b2) and (c2). Since SPR is a function of both J_d and ΔT_H ($T_{Hin} - T_{Hout}$), at high hot inlet temperatures ΔT_H increases while J_d increases even more significantly. Therefore, SPR increases with the increase in T_{Hin}. On the other hand at higher T_{Cin} the increase in SPR is not much significant compared with the effect of T_{Hin}. This is due to

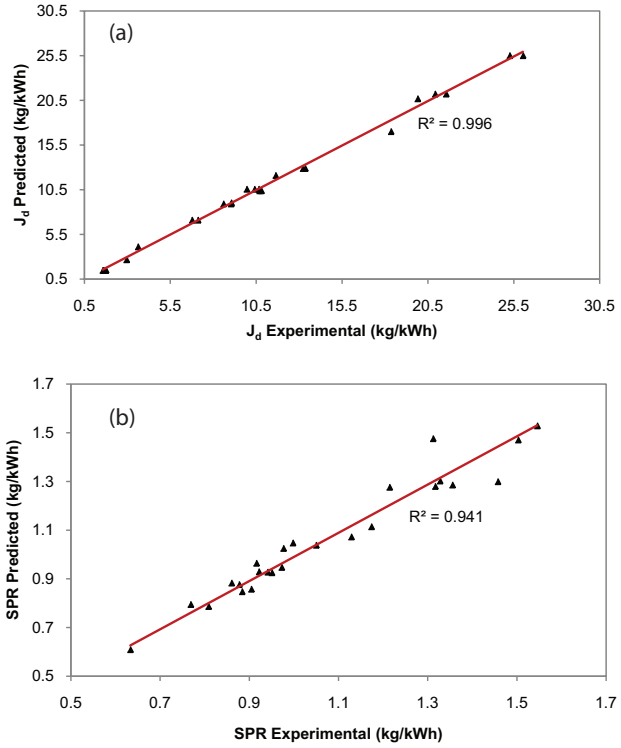

Fig. 7. Comparison between the experimental and the predicted AGMD specific performance indices determined by the RSM model. (a) Distillate flux J_d and (b) specific performance ratio (SPR).

reduction in effective driving force for distillate production at higher T_{Cin}. V_f has a negative effect on SPR because of the shorter retention time of the stream within the module which results in a lower energy recovery efficiency obtained due to less sensible heat transfer thereby decreasing the flux. From Fig. 8(c2), it can be seen that interaction effects of T_{Hin} and V_f is the most significant factor that dominated SPR.

3.3. Numerical optimization of parameters

The numerical optimization tool in design expert software was used to obtain the optimum combination of parameters for fulfilling the desired requirements. It must be noted that the optimized operational conditions for bench scale MD unit depends on the thermophysical aspects and hydrodynamic conditions which could be obtained through iterations [24]. Several solutions were provided by the simple RSM optimization, which might be helpful to control the process of MD system. For controlled operation multivariable optimization analysis has to be carried out further to maximize the performance indicators. Optimization was performed based on the data obtained from the predictive models for two responses, distillate flux (J_d) and SPR as a function of two main factors: hot inlet temperature (T_{Hin}) and feed flow rate (V_f). To predict optimum set of conditions, a new objective function named desirability was created ranging from 0 to 1 at the goal. Desirability function combines all the desired goals and maximizes the response through numerical optimization. The ultimate goal of optimization was to obtain the targeted response that simultaneously satisfies all the variable properties. In our case, we need to optimize system operating parameters T_{Hin} (50°C–80°C) and V_f (240–480 kg/h) at a fixed cold inlet temperature with targeted flux and SPR. Various solutions were obtained by the numerical optimization, however, we need to choose a best solution that could be suitable for implementation in operating real systems. In case of continuous operation, MD module operating at T_{Cin} = 25°C with minimum distillate production of 3 kg/h and SPR of 1 kg/kWh of energy consumption, following conditions need to be maintained to achieve a desirability of 1.

- MD hot inlet temperature T_{Hin} = 70°C ± 1°C and
- MD feed flow rate V_f = 415 ± 5 kg/h.

Considering application of this MD module to integrate with solar thermal system located in climatic conditions of UAE, minimum and maximum cold inlet temperatures (winter and summer) were chosen to be 20°C and 35°C, respectively. Fig. 9 provides the contours of desirability with respect to change in input parameters T_{Hin} and V_f. Present optimization is to achieve combined desirability of 1 with a targeted distillate flux of 15 kg/h m^2 and SPR equal to 1 kg/kWh. For T_{Cin} = 20°C, the system has to be operated with optimum conditions of T_{Hin} = 66°C and V_f = 388 kg/h. Similarly for T_{Hin} = 35°C optimum conditions for operation would be T_{Hin} = 76°C and V_f = 447 kg/h. Results show that delta T of 40°C–45°C should be maintained in order to achieve the desired operation. For dynamic input conditions as in the case of solar thermal integration, it is not possible to control MD hot feed temperatures and hence flow rate needs to be adjusted depending upon season of operation to achieve desired distillate production. Parametric optimization enables us to understand set of operating conditions need to be assigned to control auxiliary heating process in the absence of solar energy. An input control has to be provided to auxiliary heating system to maintain a minimum ΔT of 45°C with MD feed flow rate 6–7 L/min in order to obtain average distillate flow of 3 kg/h.

4. Simulation of solar thermal integrated MD

The RSM model developed for the single cassette MD module was validated for real-time application using a pilot scale solar thermal integrated MD system (SMD) installed in UAE [25]. The SMD system was simulated in TRNSYS tool [33] environment as shown in Fig. 10 in which previously developed RSM model was used for the MD system component. MD system determines the distillate production flow rate along with MD hot side outlet temperature. Other main components of the SMD system are the solar collectors, a heat exchanger, three pumps and a hot water storage tank. The heat exchanger transfers heat from the collectors to the MD feedwater stored in a small tank from where the feed is pumped to the MD module. Cold water is pumped to MD from a cold water storage tank having temperatures based on the ambient conditions of the location.

Table 5 shows the main specifications considered for the components for the SMD system. Five flat plate collectors having a total area of 12.75 m^2 was considered for both experiments and simulation model. For the collector tilt, a value equal to the latitude plus 10° was found to be appropriate for maximizing energy gain in winter [34]. Rate of radiation

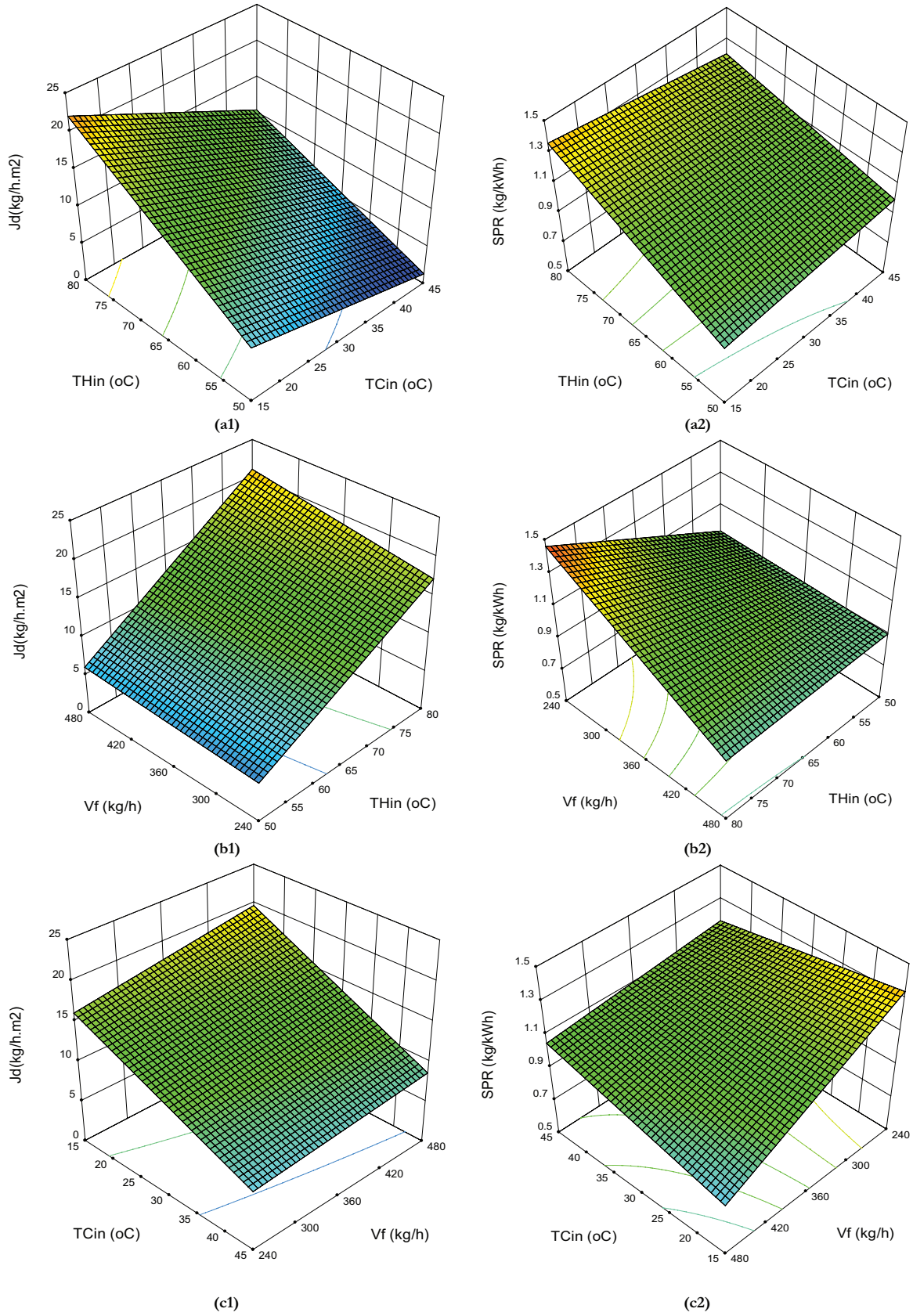

Fig. 8. 3D response surface plots of responses distillate flux (J_d) and SPR as a function of operating parameters. (a1) and (a2) J_d/SPR vs. T_{Hin} and T_{Cin} with fixed V_f; (b1) and (b2) J_d/SPR vs. V_f and T_{Cin} with fixed T_{Hin}; (c1) and (c2) J_d/SPR vs. V_f and T_{Hin} with fixed T_{Cin}.

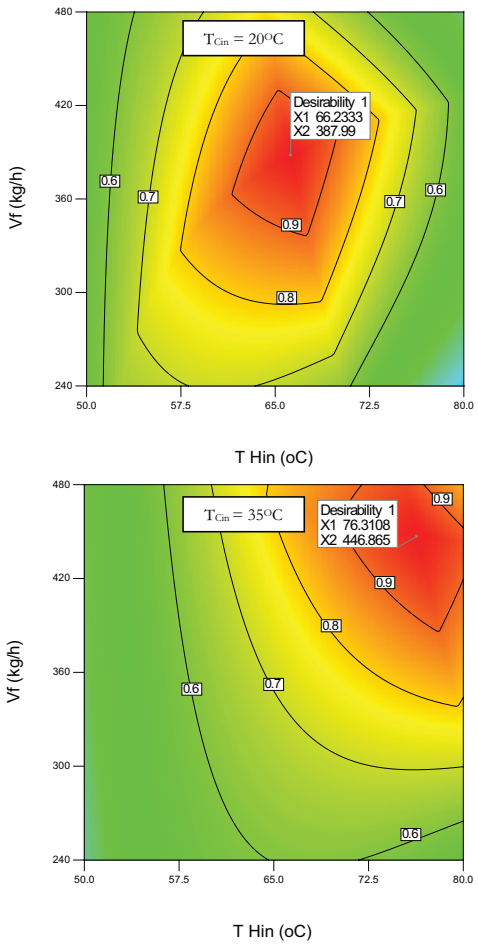

Fig. 9. Optimum operating conditions for response J_d = 15 kg/h m^2 and SPR = 1 kg/kWh at fixed cold inlet temperatures.

captured by the collectors was further increased with a south facing orientation. A simple storage tank with fixed inlets and uniform heat losses was utilized for feedwater storage. Temperature differential controller was used to control the flow of heat transfer fluids in the solar thermal system. Weather data were obtained from a weather station located in the premises of experimental system. For the experimental system, various inlet and outlet parameters were measured using temperature, flow, conductivity sensors and the data are continuously recorded. The details of the instrumentation were discussed in our previous publication [25].

Experiments on SMD system were carried out in the month of October during which maximum radiation would be incident on solar collectors installed in UAE. As shown in Fig. 11, experimental results closely follows the simulation values for MD system obtained using RSM model. The trend shows slight deviation in MD hot inlet temperatures and thereby changing distillate flow as well. Variation during peak hours of the day would be due to losses in the experimental system, which was not accounted in the simulation model. It is clearly shown in Fig. 11 that SPR trends

Table 5
Main specifications for the solar thermal integrated MD system

System component	Parameter	Value
Solar collectors (flat plate)	Area, m^2	12.75
	Collector efficiency	0.781
	Collector flow rate, kg/h m^2	25
	Tilt angle, °	35
Heat exchanger	Effectiveness	0.5
MD hot water store	Volume, L	100
MD hot pump	Flow rate, kg/h	420

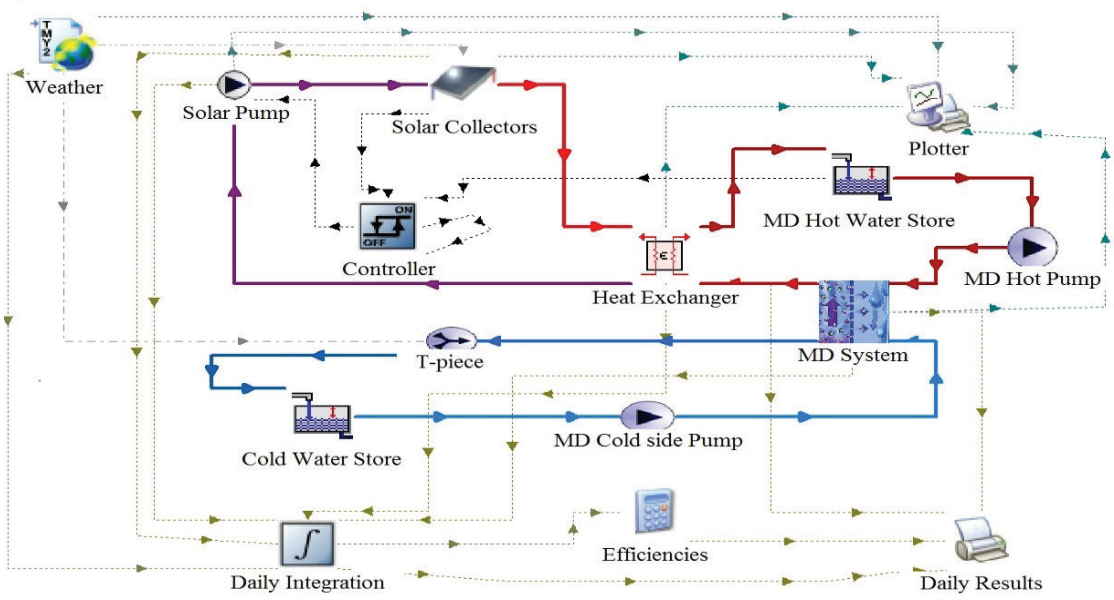

Fig. 10. Schematic flow diagram of solar membrane distillation system in TRNSYS dynamic simulation.

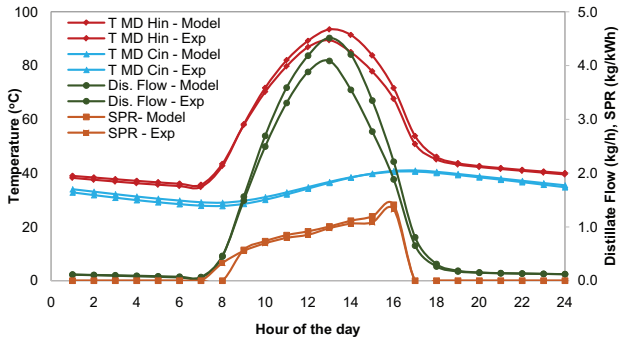

Fig. 11. Comparison of experimental data with simulation of SMD based on RSM model.

were similar in both cases due to its dependency on hot side temperature difference and flow rate rather than only inlet temperature.

5. Conclusions

A semi-commercial AGMD module is characterized experimentally. Distillate flux was varied from 0.1 to 26 L/m^2 h, with changes in different operating parameters. Higher values were achieved with high hot feed temperature and flow rates. Specific thermal energy demand values were in the range of 700–1,100 kWh/m^3, and performance ratio of less than 1 was obtained. Based on the experimentally characterized AGMD module, the relationships between operating parameters including cold feed inlet temperature, hot feed inlet temperature and feed-in flow rate and performance indicators including distillate flux and SPR taking MD energy consumption into consideration were established by RSM. Factorial DoE conducted to develop a regression model and tested by ANOVA. The model was proved valid with experimental comparisons in predicting the performance indicators. Based on the regression model and simple RSM optimization analysis the following conclusions were drawn:

- MD hot inlet temperature had the highest positive effect on flux followed by feed flow rate while cold inlet temperature had negative effect on the flux J_d. For SPR, T_{Hin} had the highest positive effect followed by T_{Cin} whereas as V_f had negative effect on SPR.
- The interaction effects between all the input parameters was evident in modeling the distillate flux whereas for SPR high variations were observed due to the interaction effects of the feed flow rate and the feed inlet temperature.
- Models showed good agreement with the experimental data fitted with second-order polynomial having determination coefficient (R^2) values of 0.996 and 0.941 for J_d and SPR, respectively.
- At an average T_{Cin} of 25°C and for production of 3 kg/h of distillate with SPR = 1 kg/kWh, optimum conditions were obtained using RSM optimization T_{Hin} = 70°C ± 1°C and V_f = 415 ± 5 kg/h.

Based on the application of integrating bench scale MD module with solar thermal system, numerical optimization has been carried out to optimize input parametric conditions for operating the system in UAE climatic conditions. For desired distillate flux of 15 kg/h m^2, MD hot and cold side temperature difference has to maintain between 40°C and 45° and flow rate needs to be adjusted from 6 to 7 L/min depending upon the season of operation. Optimized parametric conditions were used to operate pilot scale solar thermal driven membrane distillation (SMD) system in UAE and the system was simulated using TRNSYS tool. RSM model was used in the simulation studies for modeling MD system component. Dynamic simulation results of the SMD system shows good agreement with the experimental values.

References

[1] E. Drioli, A. Alib, F. Macedonio, Membrane distillation: recent developments and perspectives, Desalination, 356 (2015) 56–84.
[2] L. Eykens, K. De Sittera, C. Dotremonta, L. Pinoyc, B. Van der Bruggen, Membrane synthesis for membrane distillation: a review, Sep. Purif. Technol., 182 (2017) 36–51.
[3] A. Alkhudhiri, N. Darwish, N. Hilal, Membrane distillation: a comprehensive review, Desalination, 287 (2012) 2–18.
[4] M.S. El-Bourawi, Z. Ding, R. Ma, M. Khayet, A framework for better understanding membrane distillation separation process, J. Membr. Sci., 285 (2006) 277–282.
[5] L. Francis, N. Ghaffour, A.A. Alsaadi, G.L. Amy, Material gap membrane distillation: a new design for water vapor flux enhancement, J. Membr. Sci., 448 (2013) 240–247.
[6] M. Essalhia, M. Khayet, Application of a porous composite hydrophobic/hydrophilic membrane in desalination by air gap and liquid gap membrane distillation: a comparative study, Sep. Purif. Technol., 133 (2014) 176–186.
[7] J. Swaminathana, H.W. Chunga, D.M. Warsingera, F.A. AlMarzooqib, H.A. Arafatb, J.H. Lienhard, Energy efficiency of permeate gap and novel conductive gap membrane distillation, J. Membr. Sci., 502 (2016) 171–178.
[8] A.M. Alklaibi, N. Lior, Membrane-distillation desalination: status and potential, Desalination, 171 (2004) 111–131.
[9] L. Camacho, L. Dumée, J. Zhang, J.-d. Li, M. Duke, J. Gomez, S. Gray, Advances in membrane distillation for water desalination and purification applications, Water, 5 (2013) 94–196.
[10] A. Kullab, R. Fakhrai, A.R. Martin, Experimental evaluation of a modified air-gap membrane distillation prototype, Desal. Wat. Treat., 51 (2013) 4998–5004.
[11] J.H. Hanemaaijer, J.V. Medevoort, A.E. Jansen, Memstill membrane distillation – a future desalination technology, Desalination, 199 (2006) 175–176.
[12] G.W. Meindersma, C.M. Guijt, A.B. de Haan, Desalination and water recycling by air gap membrane distillation, Desalination, 187 (2006) 291–301.
[13] J. Koschikowski, M. Wieghaus, M. Rommel, V.S. Ortin, B.P. Suarez, J.R. Betancort Rodríguez, Experimental investigations on solar driven stand-alone membrane distillation systems for remote areas, Desalination, 248 (2009) 125–131.
[14] D. Winter, J. Koschikowski, M. Wieghaus, Desalination using membrane distillation: experimental studies on full scale spiral wound modules, J. Membr. Sci., 375 (2011) 104–112.
[15] A. Ruiz-Aguirre, D.C. Alarcón-Padilla, G. Zaragoza, Productivity analysis of two spiral-wound membrane distillation prototypes coupled with solar energy, Desal. Wat. Treat., 55 (2015) 2777–2785.
[16] N.T. Uday Kumar, A. Martin, Co-generation of drinking water and domestic hot water using solar thermal integrated membrane distillation system, Energy Procedia, 61 (2014) 2666–2669.
[17] E.U. Khan, A. Martin, Water purification of arsenic-contaminated drinking water via air gap membrane distillation (AGMD), Period. Polytech. Mech. Eng., 58 (2014) 47–53.
[18] I. Hitsov, T. Maere, K. De Sitter, C. Dotremont, I. Nopens, Modelling approaches in membrane distillation: a critical review, Sep. Purif. Technol., 142 (2015) 48–64.

[19] M. Khayet, C. Cojocaru, C. Garcia-Payo, Application of response surface methodology and experimental design in direct contact membrane distillation, Ind. Eng. Chem. Res., 46 (2007) 5673–5685.
[20] M. Khayet, C. Cojocaru, Air gap membrane distillation: desalination, modeling and optimization, Desalination, 287 (2012) 138–145.
[21] Q. He, P. Li, H. Geng, C. Zhang, J. Wang, H. Chang, Modeling and optimization of air gap membrane distillation system for desalination, Desalination, 354 (2014) 68–75.
[22] P. Onsekizoglu, K. Savas Bahceci, J. Acar, The use of factorial design for modeling membrane distillation, J. Membr. Sci., 349 (2010) 225–230.
[23] T. Mohammadi, M.A. Safavi, Application of Taguchi method in optimization of desalination by vacuum membrane distillation, Desalination, 249 (2009) 83–89.
[24] M. Khayet, C. Cojocaru, A. Baroudi, Modeling and optimization of sweeping gas membrane distillation, Desalination, 287 (2012) 159–166.
[25] N.T. Uday Kumar, A. Martin, Co-production performance evaluation of a novel solar combi system for simultaneous pure water and hot water supply in urban households of UAE, Energies, 10 (2017) 481.
[26] G. Mohan, N.T. Uday Kumar, M.K. Pokherel, A. Martin, A novel solar thermal polygeneration system for sustainable production of cooling, clean water and domestic hot water in United Arab Emirates: dynamic simulation and economic evaluation, Appl. Energy, 167 (2016) 173–188.
[27] M. Asim, N.T. Uday Kumar, A. Martin, Feasibility analysis of installation of solar combi system for simultaneous production of pure drinking water through membrane distillation desalination technique and solar domestic hot water for single family villa: a pilot plant setup in UAE, Desal. Wat. Treat., 57 (2016) 21674–21684.
[28] Scarab Development AB. Available at: http://www.scarab.se/ (Accessed March 2017).
[29] E.G. Burrieza, J. Blanco, G. Zaragoza, D.C. Alarcón, P. Palenzuela, M. Ibarra, W. Gerjak, Experimental analysis of an air gap membrane distillation solar desalination pilot plant system, J. Membr. Sci., 379 (2011) 386–396.
[30] Design Expert Software Version 10. Available at: http://www.statease.com/software.html (Accessed March 2017).
[31] A. Cipollina, M.G. di Sparti, A. Tamburini, G. Micale, Development of a membrane distillation module for solar energy seawater desalination, Chem. Eng. Res. Des., 90 (2012) 2101–2121.
[32] A. Kullab, A. Martin, Membrane distillation and applications for water purification in thermal cogeneration plants, Sep. Purif. Technol., 76 (2011) 231–237.
[33] Transient System Simulation Tool. Available at: http://www.trnsys.com/ (Accessed March 2017).
[34] N.T. Uday Kumar, A. Martin, Simulation and economic analysis of solar thermal cogeneration system for production of heat and pure water using membrane distillation, Int. J. Therm. Environ. Eng., 11 (2016) 33–39.